UV Irradiation and Humic Acid Mediate Aggregation of Aqueous Fullerene (nC_{60}) Nanoparticles

XIAOLEI QU,[†] YU SIK HWANG,*[,†] PEDRO J. J. ALVAREZ,[†] DERMONT BOUCHARD,[‡] AND QILIN LI*[,†]

Department of Civil and Environmental Engineering, Rice University, Houston Texas 77005, United States, and U.S. Environmental Protection Agency, National Exposure Research Laboratory, Athens Georgia 30605, United States

Received June 8, 2010. Revised manuscript received September 10, 2010. Accepted September 13, 2010.

The transport and fate of engineered nanomaterials is affected by multiple environmental factors, including sunlight and natural organic matter. In this study, the initial aggregation kinetics of aqueous fullerene (nC_{60}) nanoparticles before and after UVA irradiation was investigated in solutions varying in ionic strength, ionic composition, and humic acid concentration. In NaCl solutions, surface oxidation induced by UV irradiation remarkably increased nC_{60} stability due to the increased negative surface charge and reduced particle hydrophobicity; although humic acid greatly enhanced the stability of pristine nC_{60} via the steric hindrance effect, it had little influence on the stability of UV-irradiated nC_{60} in NaCl due to reduced adsorption on oxidized nC_{60} surface. In contrast, UV irradiation reduced nC_{60} stability in $CaCl_2$ due to specific interactions of Ca^{2+} with the negatively charged functional groups on UV-irradiated nC_{60} surface and the consequent charge neutralization. By neutralizing surface charges of both UV-irradiated nC_{60} and humic acid as well as forming intermolecular bridges, Ca^{2+} facilitated humic acid adsorption on UV-irradiated nC_{60}, resulting in enhanced stability in the presence of humic acid. These results demonstrate the critical role of nC_{60} surface chemistry in its environmental transport and fate.

Introduction

C_{60} fullerene has drawn much attention due to its potential applications in various fields including optics, cosmetics, and pharmaceuticals (*1*−*4*). Despite its extremely low water solubility, C_{60} readily forms stable nanosized particles in water, usually referred to as nC_{60}, by solvent exchange, sonication, or extended stirring (*5*−*9*). The relatively high bioavailability and "solubility" of nC_{60} have raised concern regarding its potential health impact to human and ecological systems through environmental exposure; evidence of toxicity has been reported in a number of studies showing production of reactive oxygen species or cell oxidation upon direct contact (*10*−*13*). Aggregation is an important process governing the mobility and toxicity of nC_{60} (*13*−*17*). nC_{60} aggregation behavior in different electrolyte solutions has been quantitatively studied (*18*−*20*). These studies suggest that pristine nC_{60} stability can be adequately described by the traditional Derjaguin−Landau−Verwey−Overbeek (DLVO) theory (*21, 22*). Compared to monovalent cations, divalent cations are much more efficient in coagulating nC_{60} as described by the Schulze−Hardy Rule (*19, 23*).

Natural organic matter (NOM), ubiquitous in aquatic environments and soils, is one of the key factors governing the environmental transport and fate of colloids. NOM can adsorb onto colloidal particles, alter their surface properties and consequently affect their transport patterns. The capability of adsorbed NOM to stabilize colloids such as nC_{60}, hematite, magnetite, and clay particles is well recognized (*19, 24*−*26*). The steric hindrance effect has been reported to be responsible for the enhanced nC_{60} stability in the presence of humic acid (*19*).

Because nC_{60} can remain suspended for an extended period of time at the ionic strength and pH found in surface waters (*20, 27*), exposure to sunlight could be an important process that affects its environmental fate. C_{60} has strong light absorption within the solar spectrum, especially in the UV range. Recent studies demonstrated that nC_{60} undergoes surface modification or decomposition under sunlight or UV irradiation (*7, 28, 29*). Oxygen-containing functional groups were identified on the irradiated nC_{60} particle surface. These studies suggest that surface-oxidized nC_{60} may be an important form of C_{60} in the aquatic environment. In addition, a recent study on the aggregation behavior of multiwalled carbon nanotubes (MWCNTs) suggests that oxygen-containing surface functional groups may have a great impact on the aggregation of carbon nanomaterials. A positive linear relationship was found between the critical coagulation concentration (CCC) of the MWCNT and its total oxygen content (*30*). However, little is known about the transport of photochemically modified nC_{60}.

The objective of this study was to determine the effect of solar irradiation on the aggregation kinetics of nC_{60}. Exposure of nC_{60} to sunlight was simulated by UVA irradiation and its impact on nC_{60} aggregation was investigated in solutions varying in total ionic strength, cationic species, and organic content. To our knowledge, this is the first paper to report on the aggregation behavior of nC_{60} photochemically modified by sunlight. Our results suggest that sunlight may play a critical role in the environmental fate and transport of C_{60}.

Materials and Methods

Materials. Sublimed C_{60} powder (purity greater than 99%) was obtained from Materials Electronics Research Corporation (Tucson, AZ). Suwannee River humic acid standard (II) (SRHA, International Humic Substances Society, Atlanta, GA) was used as the surrogate for aquatic NOM. The SRHA powder (100 mg) was dissolved in 100 mL of DI water and stirred for 24 h in dark. The pH was adjusted to 8.5 with NaOH to aid the dissolution of SRHA. The stock solution was then filtered through 0.45-μm pore-size Whatman membrane filters to remove undissolved SRHA. The concentration of the stock solution, 894 mg/L (470 mg/L as carbon), was determined by total organic carbon (TOC) analysis using a high-sensitivity TOC analyzer (Shimadzu Scientific Instruments, Columbia, MD) based on the carbon content (52.6%) of SRHA (*31*). Reagent-grade NaCl and $CaCl_2$ were obtained from Aldrich Chemicals (Milwaukee, WI).

Preparation of nC_{60} Stock Suspension. The aqueous nC_{60} stock suspension was prepared by direct sonication (*7*). Sublimed C_{60} was pulverized into fine powder and 150 mg

* Address correspondence to either author. Q.L. phone: (713)348-2046; fax: (713)348-5268; e-mail: qilin.li@rice.edu. Y.S.H. phone: (713)348-5794; e-mail: hwangyusik@gmail.com; present address: Graduate School of Energy and Environmental System Engineering, University of Seoul, Seoul 130-743, Korea.

[†] Rice University.

[‡] U.S. Environmental Protection Agency.

10.1021/es101947f
Published on Web 09/24/2010

of this powder was added to 200 mL of deionized water in a 500-mL glass beaker. The mixture was then put in an ice bath and sonicated with a sonicating probe (Vibra-Cell VCX 500, Sonics & Material, Newtown, CT) at 100 W for 30 min. After sonication, the mixture was filtered through 2-μm pore-size Millex-AP membrane filters (Millipore, Billerica, MA) to remove large particles. All filters were washed with 10 mL of DI water before use and replaced after 30 mL of filtrate was collected. The resulting clear yellow suspension was stored in dark at 4 °C until use. The C_{60} concentration in the stock suspension was 4.4 mg/L as determined by TOC measurement. All experiments were performed using the same stock suspension. Particle size of the stock suspension was routinely monitored over the period of the study (3 months); there were no detectable changes.

Irradiation Experiments. Irradiation experiments were carried out in a Luzchem LZC-4 V photoreactor (Luzchem, Ottawa, Ontario, Canada). Because UVA is the primary component of UV light in the solar irradiation that can reach the earth surface, a light source in the UVA wavelength range was employed to mimic the UV fraction of the solar spectrum. Four 8-W black lamps (Hitachi FL8BL-B, $\lambda = 350 \pm 50$ nm), two on each side, provided approximately 2 mW/cm^2 (1.66 mW/cm^2 after absorption by the sample flask) of light intensity at the center of the reactor as measured by a radiometer (Control Company, Friendwoods, TX), comparable to the UVA intensity measured at the ground level on a sunny summer day in Houston, TX. In each experiment, 30 mL of the nC_{60} stock suspension at unadjusted pH 6.3 was added to a 50-mL Erlenmeyer flask, sealed with parafilm with vents, placed on the merry-go-round at the center of the photoreactor, and slowly rotated to ensure uniform exposure. Samples were withdrawn on days 1, 2, 3, and 7, and stored in dark at 4 °C before testing.

Physical and chemical properties of the irradiated nC_{60} suspension were thoroughly characterized by transmission electron microscopy (TEM), X-ray photoelectron spectroscopy (XPS), attenuated total reflectance Fourier transform infrared (ATR-FTIR) spectroscopy, and UV/vis spectroscopy as reported in our previous study (*7*).

Characterization of Particle Size and Electrophoretic Mobility. Particle sizes of the pristine and irradiated nC_{60} were determined by dynamic light scattering (DLS) measurement using a ZEN 3600 Zetasizer Nano (Malvern, Worcestershire, UK) equipped with a monochromatic coherent He−Ne laser with a fixed wavelength of 633 nm. The intensity of scattered light was measured at 173° and the refractive index of nC_{60} was set at 2.20 (*9*). Each sample was measured 6 times consecutively for the hydrodynamic radius. Particle electrophoretic mobility (EPM) was measured by phase analysis light scattering (PALS) using the ZEN 3600 Zetasizer Nano (Malvern, Worcestershire, UK). Measurements were carried out using folded capillary cells (Malvern, Worcestershire, UK) and 10 measurements were made for each sample. All size and EPM measurements were conducted at 23 °C.

nC_{60} Aggregation Kinetics. *Measurement of Particle Aggregation Rate*. Aggregation of the pristine and irradiated nC_{60} suspensions in various solution conditions was characterized by monitoring the intensity weighted average particle size as a function of time via time-resolved DLS measurement. For experiments without humic acid, 0.25 mL of the nC_{60} stock suspension, predetermined amount of the electrolyte stock solution, and DI water were introduced into a disposable polystyrene cuvette (Sarstedt, Germany) to create a sample with a total volume of 1 mL and nC_{60} concentration of 1.1 mg/L. The sample was briefly mixed and immediately analyzed. The autocorrelation function was applied to data collected every 15 s. Since initiation of the instrument took 1 min, the first particle size datum was collected at 75 s after the nC_{60} suspension was mixed with the electrolyte solution.

For most experiments with humic acid, 5 mL of nC_{60} stock suspension was precontacted with 5 mL of SRHA solution at the same concentration as that used in the subsequent DLS measurement in a glass vial on a shaker bed for 24 h to allow adsorption. This mixture was then combined with the background solution containing the corresponding electrolyte and SRHA to form samples with 1.1 mg/L nC_{60} and 1 mg/L or 10 mg/L SRHA in 1 mL total volume. Selected experiments were also performed without SRHA precontact and compared with those with precontact to investigate the impact of SRHA adsorption dynamics.

Determination of Aggregation Kinetics. The rate of initial increase in the intensity weighted average hydrodynamic radius $a_h(t)$ determined by linear regression of the aggregation curve was used to represent the initial aggregation rate. Details of the data analysis and an example of the raw aggregation data (Figure S1) can be found in the Supporting Information (SI). Extrapolation of the aggregation data to time zero shows that the estimated particle size at time zero was similar for all experiments (average 86.5 ± 2.8 nm in NaCl and 86.9 ± 2.1 nm in $CaCl_2$; Figure S2) and close to that measured in DI water (82.3 ± 0.9 nm). This indicates that there were no significant changes in aggregation rate in the first 75 s, during which particle size data were not available, suggesting that the aggregation rate obtained represents the initial aggregation rate.

The attachment efficiency α is defined as the aggregation rate constant in the solution of interest normalized by the rate constant in the diffusion-limited regime, where the aggregation rate constant is independent of electrolyte concentration (*18*). In our analysis, the diffusion-limited aggregation rate was determined by averaging the aggregation rates of all aggregation kinetic curves obtained in the diffusion-limited regime. Stability curves were constructed by plotting the α value as a function of the background electrolyte concentration. For easy comparison, the diffusion-limited aggregation rate determined for the pristine nC_{60} in the absence of SRHA was used as the diffusion-limited aggregation rate for all the stability curves in the same electrolyte. The critical coagulation concentration (CCC) was approximated by the electrolyte concentration at the intersection of the reaction-limited stability curve and the diffusion-limited stability curve (as shown in Figures 1 and 4).

Result and Discussion

Characterization of nC_{60} Nanoparticles. The number mean and Z-average hydrodynamic radii of the pristine nC_{60} suspension were 54.8 ± 2.4 nm and 82.3 ± 0.9 nm, respectively. The particles were highly negatively charged with an electrophoretic mobility of $-3.34 \pm 0.13 \times 10^{-8}$ m^2 V^{-1} s^{-1} in 1 mM NaCl. The surface chemical properties of irradiated nC_{60} suspension prepared using the same protocol were thoroughly characterized in our previous study (*7*). Mono-oxygenated carbon (C−O) and dioxygenated carbon (C═O or O−C−O) accounted for 19 and 15%, respectively, of the total carbon on the 7-day irradiated-nC_{60} surface. ATR-FTIR analyses confirmed surface oxygenation and hydroxylation. After 7 days of UVA irradiation, both the number mean particle size in DI water (54.7 ± 3.6 nm) and the electrophoretic mobility in 1 mM NaCl ($-3.24 \pm 0.19 \times 10^{-8}$ m^2 V^{-1} s^{-1}) remained unchanged, consistent with previous results (*7*). The unchanged particle size suggests that there was no significant release of photochemical oxidation products into the aqueous phase, and the number concentration of nC_{60} was assumed to remain unchanged.

Aggregation Kinetics in NaCl Solutions. The attachment efficiency (α) of nC_{60} in NaCl solutions before and after UV

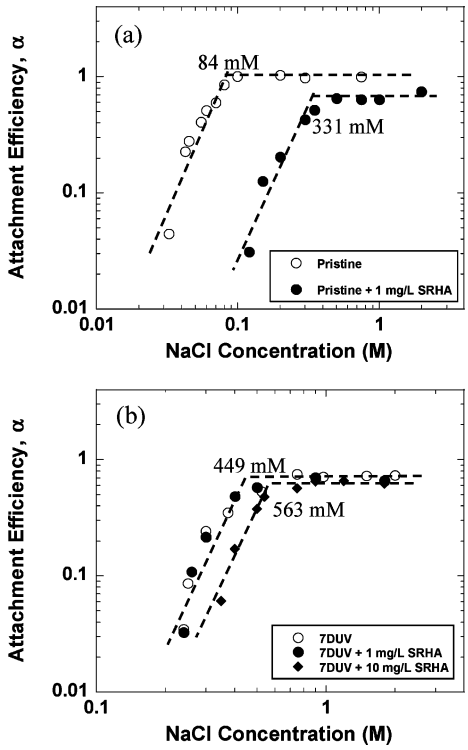

FIGURE 1. Attachment efficiencies of (a) pristine nC_{60} and (b) 7-day UV-irradiated nC_{60} (7DUV) in the absence and presence of SRHA as a function of NaCl concentration at pH 6.0 ± 0.3. Extrapolation of the reaction-limited and diffusion-limited regimes yields the critical coagulation concentrations (CCC) at the intersections. The CCC values are noted next to the corresponding intersection.

irradiation is shown in Figure 1. The pristine nC_{60} nanoparticles were stable only at NaCl concentrations below 20 mM, with a CCC of 84 mM. Our CCC value is lower than those previously reported for nC_{60} prepared by solvent exchange (160 mM NaCl (*19*) and 120 mM NaCl (*18*)) or by magnetic stirring (260 mM NaCl (*32*) and 166 mM KCl (*20*)), but higher than that (40 mM KCl (*20*)) of another sonicated nC_{60} that was dissolved in toluene before sonication. After 7 days of UVA irradiation, the stability of nC_{60} nanoparticles (denoted 7DUV-nC_{60}) in NaCl increased drastically (Figure 1b), with a CCC of 449 mM NaCl.

The nC_{60} aggregation rate decreased with increasing UV irradiation time during the 7-day period. Figure 2 demonstrates the effect of UV irradiation time on the aggregation kinetics of nC_{60} in 300 mM NaCl. After 7 days of UVA irradiation, the initial aggregation rate dropped from 0.110 to 0.024 nm/s. Such increase in stability is attributed to the presence of oxygen-containing functional groups on the surface of the irradiated nC_{60} particles (*7, 29*). Similar effects of surface oxygen-containing functional groups were reported for nC_{60} prepared by long-term stirring and carbon nanotubes oxidized by acid wash; these effects were related to the extent of surface oxidation and resulting changes in surface charge or electrophoretic mobility (*20, 30, 33*).

The electrophoretic mobility of nC_{60} before and after UVA irradiation at different NaCl concentrations is compared in Figure 3a. For both the pristine and UV irradiated samples, particle electrophoretic mobility became less negative with increasing NaCl concentration due to charge screening. The pristine nC_{60} and 7DUV-nC_{60} were similarly charged at NaCl concentrations below 10 mM; in the NaCl concentration range of 10−200 mM; however, the 7DUV-nC_{60} surface was notably more negatively charged than the pristine nC_{60}, consistent with the higher colloidal stability. The difference

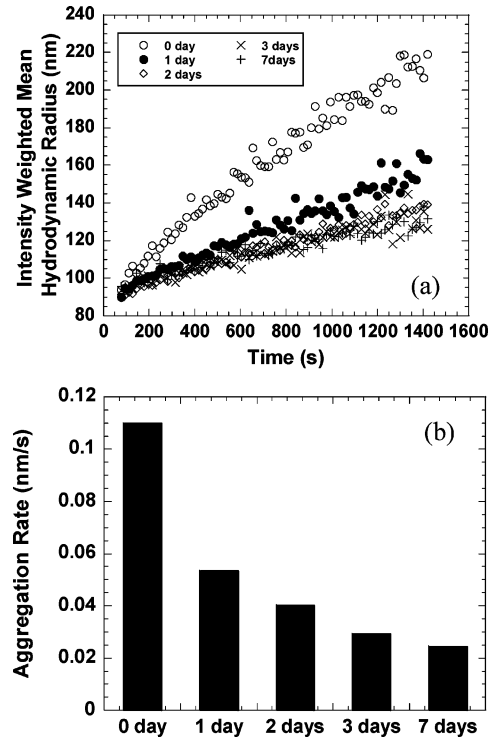

FIGURE 2. (a) Aggregation profiles and (b) initial aggregation rates of samples with different UV irradiation time in 300 mM NaCl at pH 6.0 ± 0.3.

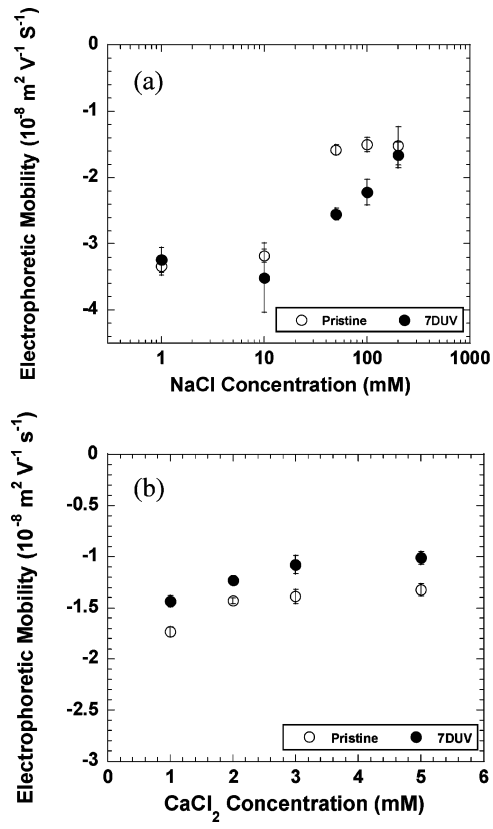

FIGURE 3. Electrophoretic mobility of pristine nC_{60} and 7-day UV-irradiated nC_{60} (7DUV) as a function of (a) NaCl and (b) $CaCl_2$ concentration at pH 6.0 ± 0.3.

in response to the charge screening effect of NaCl is attributed to the changes in nC_{60} surface chemistry; i.e., addition of oxygen-containing functionalities, during UV irradiation. Differences in electrophoretic mobility were also reported

for nC_{60} samples prepared by different protocols (*9*), and were attributed to differences in surface chemistry. A close examination of the electrophoretic mobility data reveals that changes in particle electrophoretic mobility alone could not account for the observed increase in particle stability after UV irradiation. For example, the electrophoretic mobility of the 7DUV-nC_{60} in 200 mM NaCl was $-1.66 \pm 0.19 \times 10^{-8}$ m^2 V^{-1} s^{-1}, similar to that of the pristine nC_{60} at its CCC of 84 mM NaCl, where rapid aggregation occurred. Nevertheless, the 7DUV-nC_{60} was very stable with an α value less than 0.001 in 200 mM NaCl. Such inconsistency between the electrophoretic mobility and the stability of nanoparticles has also been reported in previous studies on multiwalled carbon nanotubes (MWCNTs). Smith et al. (*30, 33*) found that although the CCCs of oxidized MWCNTs increased with increasing surface oxidation, the changes in electrophoretic mobility did not correlate well to the CCCs. This discrepancy was attributed to the fact that electrophoretic mobility reflects the potential at the plane of shear, not the actual surface charge (*30*). Another possible reason is that the surface oxygen-containing functional groups increased nC_{60} hydrophilicity and decreased hydrophobic interactions, as described by the extended DLVO theory (*34*).

As a major component of NOM, humic acid is ubiquitous in the natural aqueous environment. It has a heterogeneous structure with hydrophobic backbones and hydrophilic side chains. Although negatively charged, humic acid can readily adsorb onto colloidal surfaces such as that of nC_{60} via hydrophobic interaction, potentially mediating colloidal aggregation. The capability of adsorbed NOM to stabilize colloids like nC_{60}, hematite, magnetite, and clay particles is widely reported (*19, 24*−*26*). As shown in Figure 1a, SRHA at 1 mg/L greatly increased the stability of the pristine nC_{60}; the CCC increased from 84 to 331 mM NaCl. On the other hand, the electrophoretic mobility of nC_{60} did not change notably after equilibrating with 1 mg/L SRHA, suggesting that electrostatic interactions were not responsible for the increase in stability. This is consistent with the finding of Chen and Elimelech (*19*). The increased stability in the presence of SRHA is attributed to the steric hindrance effect of humic acid molecules adsorbed on the nC_{60} surface. With 10 mg/L SRHA, no aggregation of pristine nC_{60} was observed at NaCl concentrations up to 1.5 M NaCl within 20 min (data not shown). This further demonstrates that steric hindrance rather than electrostatic repulsion is the main stabilizing mechanism in the presence of humic acid, since the surface charge should be effectively screened at such an elevated NaCl concentration.

The effect of humic acid on the stability of 7DUV-nC_{60} (Figure 1b) was much weaker. At 1 mg/L SRHA, there was no notable change in particle stability; when SRHA concentration was increased to 10 mg/L, particle stability increased slightly with a CCC of 563 mM compared to 449 mM without humic acid. The small influence of humic acid on the aggregation properties of 7DUV-nC_{60} is attributed to decreased adsorption of humic acid due to increased hydrophilicity of the nC_{60} surface after UV irradiation, as demonstrated in Table S1 in the Supporting Information. Unlike pristine nC_{60}, which showed significant adsorption of SRHA ($q = 1209$ mg/kg), UV-irradiated nC_{60} had no detectable adsorption of SRHA during 24 h of contact. These results suggest that the stability of the UV-irradiated nC_{60} depends more on the oxygen-containing surface functional groups than humic acid, and the role of humic acid may be further reduced at longer irradiation time, which increases the level of surface oxidation (*7*).

Attachment efficiencies in the diffusion-limited regime of the pristine nC_{60} with humic acid ($\alpha = 0.66$) and the 7DUV-nC_{60} with ($\alpha = 0.68$) and without humic acid ($\alpha = 0.73$) were found to be less than unity. The decrease in α in the diffusion-limited regime was reported previously with humic acid in $MgCl_2$ solutions (*19*) and indicates that the steric hindrance effect, which cannot be eliminated by double layer compression, predominates in stabilizing the pristine nC_{60} at high NaCl concentrations. In the absence of humic acid, however, the less-than-unity α value of the 7DUV-nC_{60} in the diffusion-limited regime indicates that the oxygen-containing surface functional groups formed during UV irradiation can stabilize nC_{60} through mechanisms not eliminated by high NaCl concentration, e.g., increase in surface hydrophilicity.

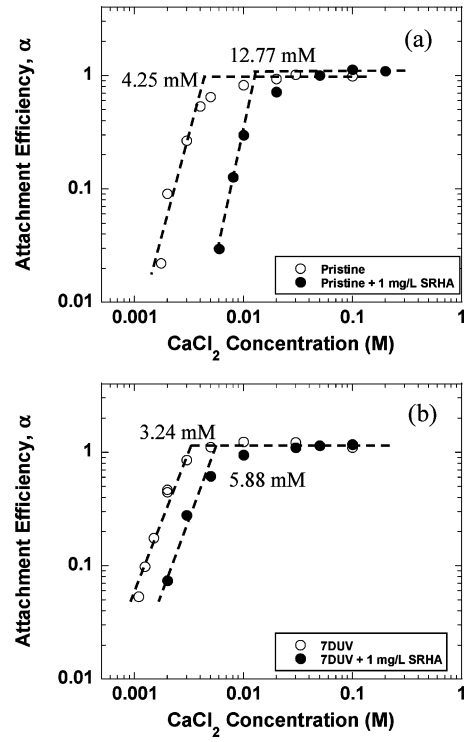

FIGURE 4. Attachment efficiencies of (a) pristine nC_{60} and (b) 7-day UV-irradiated nC_{60} (7DUV) in the absence and presence of SRHA as a function of $CaCl_2$ concentration at pH 6.0 ± 0.3. Intersections of the extrapolated lines through reaction-limited and diffusion-limited regimes yield critical coagulation concentrations, whose values are noted next to the corresponding intersections.

Aggregation Kinetics in $CaCl_2$ Solutions. Colloidal stability depends strongly on the electrolyte valence, as described by the Schulze−Hardy Rule (*23*). Cations of higher valence are more efficient in coagulation. As a result, the CCCs of $CaCl_2$ for the pristine and 7DUV-nC_{60}, 4.25 and 3.24 mM $CaCl_2$, respectively, were markedly lower than those of NaCl. Contrary to the observations in NaCl solutions, the 7DUV-nC_{60} was less stable than the pristine nC_{60} in $CaCl_2$ solutions (Figure 4). Comparison between the electrophoretic mobility of the pristine and the 7DUV-nC_{60} reveals that the 7DUV-nC_{60} was less negatively charged than the pristine nC_{60} over the entire tested range of $CaCl_2$ concentrations (Figure 3b), suggesting that Ca^{2+} was more effective in neutralizing negative charges on the 7DUV-nC_{60} surface than on the pristine nC_{60}. The Schulze−Hardy Rule predicts that the CCC is proportional to Z^{-6} (Z is the valence of the counterion) for surfaces of high charge density (*35*) and Z^{-2} for surfaces of low charge density (*36*). In our experiments, the power term is −4.3 for the pristine nC_{60} and −7.1 for the 7DUV-nC_{60}. The behavior of the pristine nC_{60} agrees with the Schulze−Hardy Rule, while the power term for the 7DUV-nC_{60} is higher than the normal range. Because the Schulze−Hardy Rule holds for indifferent electrolytes that do not form any specific interactions with the colloidal surface, this result indicates that Ca^{2+} specifically interacts with the 7DUV-nC_{60} surface, presumably with carboxyl groups formed from UV irradiation.

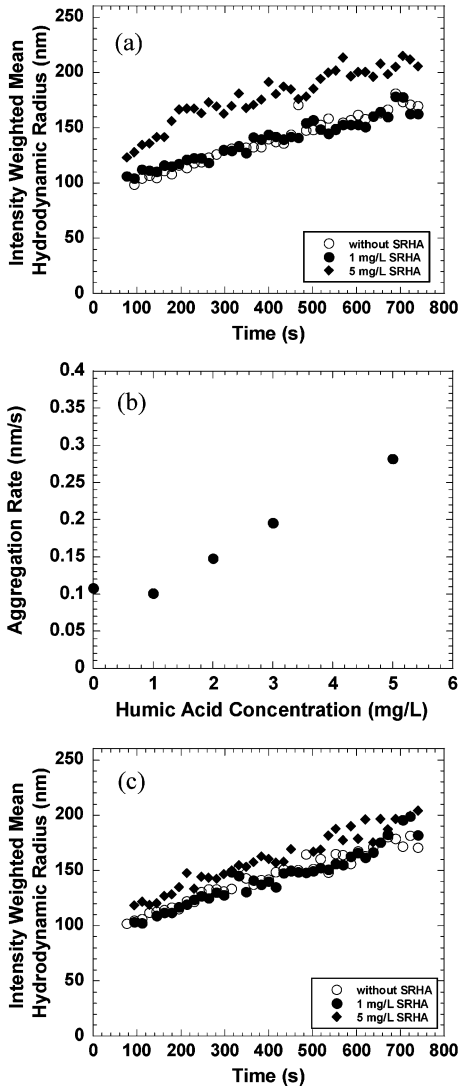

FIGURE 5. (a) Aggregation profiles of pristine nC_{60} in the absence and presence of humic acid without precontact; (b) initial aggregation rates of pristine nC_{60} as a function of humic acid concentration without precontact; and (c) aggregation profiles of pristine nC_{60} in the absence and presence of humic acid with 24 h precontact. Measurements were conducted in 200 mM $CaCl_2$.

The presence of humic acid increased the stability of the pristine nC_{60}, similar to that observed in NaCl solutions. With 1 mg/L SRHA, the CCC for the pristine nC_{60} increased from 4.25 to 12.77 mM $CaCl_2$. This is attributed to the steric hindrance effect of the adsorbed humic acid. The 7DUV-nC_{60}, however, behaved differently in $CaCl_2$ than in NaCl solutions: With 1 mg/L humic acid, the CCC increased from 3.24 to 5.88 mM $CaCl_2$, indicating adsorption of humic acid on the 7DUV-nC_{60} particle surface; the effect of humic acid at the same concentration in NaCl solutions was undetectable. This suggests that Ca^{2+} may have facilitated humic acid adsorption onto the 7DUV-nC_{60} surface. Enhanced humic acid adsorption could occur through two potential mechanisms: (1) Ca^{2+} specifically interacts with the oxygen-containing function groups (e.g., carboxyl groups) on the 7DUV-nC_{60} surface, neutralizing surface negative charges as demonstrated by the less negative EPM (Figure 3b); it complexes with humic acid and reduces its molecular charge (*37*). Consequently, the electrostatic repulsion between the 7DUV-nC_{60} and humic acid is reduced, favoring humic acid adsorption. (2) Ca^{2+} could form ionic bridges between humic acid and the oxygen-containing functional groups on the 7DUV-nC_{60}, an effect that has been reported in studies on humic acid adsorption onto mineral surfaces (*38*−*41*).

The dynamics of the contact between nC_{60} and humic acid was found to affect the aggregation behavior in the diffusion-limited regime. Figure 5 compares the aggregation rate of SRHA precoated pristine nC_{60} and that of nC_{60} simultaneously mixed with SRHA and the background $CaCl_2$ solution. All the experiments were conducted in 200 mM $CaCl_2$ to ensure that the aggregation was diffusion-limited. When pristine nC_{60} and SRHA at a concentration higher than 1 mg/L were introduced to the $CaCl_2$ solution simultaneously just before DLS measurement, the nC_{60} aggregation rate was significantly higher than that in the absence of SRHA (Figure 5a) and the initial aggregation rate increased with increasing SRHA concentration (Figure 5b). A similar effect was reported in a previous study (*19*) using nC_{60} synthesized by solvent exchange, and was attributed to the bridging of nC_{60} by humic acid aggregates. Interestingly, when the pristine nC_{60} was precontacted with SRHA for 24 h, the diffusion-limited aggregation rate was independent of SRHA concentration (Figure 5c). These results suggest that SRHA aggregation in the presence of Ca^{2+} is faster than SRHA adsorption onto nC_{60} and that once precoated with humic acid, nC_{60} does not attach to humic acid aggregates.

Environmental Implication. As demonstrated in this study, solar irradiation could play a critical role in the aggregation behavior of nC_{60} and consequently its environmental fate and transport. While the stability of the pristine nC_{60} is largely controlled by the humic acid adsorbed on the nC_{60} surface, humic acid adsorption is mediated by the oxygen-containing surface functionality on the UV-irradiated nC_{60} particles. On the other hand, the extent of nC_{60} photochemical transformation is strongly influenced by humic acid (*7*). In addition, specific interactions between cationic species such as Ca^{2+} and nC_{60} surface functionality resulting from UV irradiation or humic acid adsorption can be a dominating factor in nC_{60} aggregation kinetics. These findings suggest that a better quantitative understanding of the dynamics of nC_{60} surface chemistry change is critical to predicting fullerene transport and fate in the aqueous environment as well as risk assessment for carbon based nanomaterials.

Acknowledgments

This work was supported by the NSF Center for Biological and Environmental Nanotechnology (Award EEC-0647452) and the USEPA STAR program (Grant 834093).

Supporting Information Available

Details of (1) aggregation kinetics data analysis including determination of the initial aggregation rate, the extrapolated initial particle size, attachment efficiency, and critical coagulation concentration, and (2) SRHA adsorption experiments. This material is available free of charge via the Internet at http://pubs.acs.org.

Literature Cited

(1) Friedman, S. H.; Decamp, D. L.; Sijbesma, R. P.; Srdanov, G.; Wudl, F.; Kenyon, G. L. Inhibition of the HIV-1 Protease by Fullerene Derivatives-Model-Building Studies and Experimental-Verification. *J. Am. Chem. Soc.* **1993**, *115*, 6506–6509.

(2) Nakamura, E.; Isobe, H. Functionalized fullerenes in water. The first 10 years of their chemistry, biology, and nanoscience. *Acc. Chem. Res.* **2003**, *36*, 807–815.

(3) Cravino, A.; Sariciftci, N. S. Double-cable polymers for fullerene based organic optoelectronic applications. *J. Mater. Chem.* **2002**, *12*, 1931–1943.

(4) Burangulov, N.; Moravsky, A. P.; Kulikova, Y. V.; Dyachuk, G. I.; Loutfy, R. O. Cosmetic compositions containing fullerene clusters. U.S. Patent Application 20050136079, 2005.

(5) Xie, B.; Xu, Z. H.; Guo, W. H.; Li, Q. L. Impact of natural organic matter on the physicochemical properties of aqueous C-60 nanoparticles. *Environ. Sci. Technol.* **2008**, *42*, 2853–2859.

(6) Li, Q. L.; Xie, B.; Hwang, Y. S.; Xu, Y. J. Kinetics of C-60 Fullerene Dispersion in Water Enhanced by Natural Organic Matter and Sunlight. *Environ. Sci. Technol.* **2009**, *43*, 3574–3579.
(7) Hwang, Y. S.; Li, Q. L. Characterizing Photochemical Transformation of Aqueous nC(60) under Environmentally Relevant Conditions. *Environ. Sci. Technol.* **2010**, *44*, 3008–3013.
(8) Brant, J.; Lecoanet, H.; Hotze, M.; Wiesner, M. Comparison of electrokinetic properties of colloidal fullerenes (n-C-60) formed using two procedures. *Environ. Sci. Technol.* **2005**, *39*, 6343–6351.
(9) Brant, J. A.; Labille, J.; Bottero, J. Y.; Wiesner, M. R. Characterizing the impact of preparation method on fullerene cluster structure and chemistry. *Langmuir* **2006**, *22*, 3878–3885.
(10) Lyon, D. Y.; Brunet, L.; Hinkal, G. W.; Wiesner, M. R.; Alvarez, P. J. J. Antibacterial activity of fullerene water suspensions (nC(60)) is not due to ROS-mediated damage. *Nano Lett.* **2008**, *8*, 1539–1543.
(11) Fang, J. S.; Lyon, D. Y.; Wiesner, M. R.; Dong, J. P.; Alvarez, P. J. J. Effect of a fullerene water suspension on bacterial phospholipids and membrane phase behavior. *Environ. Sci. Technol.* **2007**, *41*, 2636–2642.
(12) Oberdorster, E. Manufactured nanomaterials (Fullerenes, C-60) induce oxidative stress in the brain of juvenile largemouth bass. *Environ. Health Perspect.* **2004**, *112*, 1058–1062.
(13) Sayes, C. M.; Gobin, A. M.; Ausman, K. D.; Mendez, J.; West, J. L.; Colvin, V. L. Nano-C-60 cytotoxicity is due to lipid peroxidation. *Biomaterials* **2005**, *26*, 7587–7595.
(14) Sayes, C. M.; Fortner, J. D.; Guo, W.; Lyon, D.; Boyd, A. M.; Ausman, K. D.; Tao, Y. J.; Sitharaman, B.; Wilson, L. J.; Hughes, J. B.; West, J. L.; Colvin, V. L. The differential cytotoxicity of water-soluble fullerenes. *Nano Lett.* **2004**, *4*, 1881–1887.
(15) Zhu, S. Q.; Oberdorster, E.; Haasch, M. L. Toxicity of an engineered nanoparticle (fullerene, C-60) in two aquatic species, Daphnia and fathead minnow. *Mar. Environ. Res.* **2006**, *62*, S5–S9.
(16) Lyon, D. Y.; Adams, L. K.; Falkner, J. C.; Alvarez, P. J. J. Antibacterial activity of fullerene water suspensions: Effects of preparation method and particle size. *Environ. Sci. Technol.* **2006**, *40*, 4360–4366.
(17) Fortner, J. D.; Lyon, D. Y.; Sayes, C. M.; Boyd, A. M.; Falkner, J. C.; Hotze, E. M.; Alemany, L. B.; Tao, Y. J.; Guo, W.; Ausman, K. D.; Colvin, V. L.; Hughes, J. B. C-60 in water: Nanocrystal formation and microbial response. *Environ. Sci. Technol.* **2005**, *39*, 4307–4316.
(18) Chen, K. L.; Elimelech, M. Aggregation and deposition kinetics of fullerene (C-60) nanoparticles. *Langmuir* **2006**, *22*, 10994–11001.
(19) Chen, K. L.; Elimelech, M. Influence of humic acid on the aggregation kinetics of fullerene (C-60) nanoparticles in monovalent and divalent electrolyte solutions. *J. Colloid Interface Sci.* **2007**, *309*, 126–134.
(20) Chen, K. L.; Elimelech, M. Relating Colloidal Stability of Fullerene (C-60) Manoparticles to Nanoparticle Charge and Electrokinetic Properties. *Environ. Sci. Technol.* **2009**, *43*, 7270–7276.
(21) Verwey, E. J. W. Theory of the Stability of Lyophobic Colloids. *Philips Res. Rep.* **1945**, *1*, 33–49.
(22) Derjaguin, B.; Landau, L. Theory of stability of highly charged liophobic sols and adhesion of highly charged particles in solutions of electrolytes. *Zhurnal Eksperimentalnoi Teor. Fiz.* **1945**, *15*, 663–682.
(23) Hardy, W. B. A preliminary investigation of the conditions which determine the stability of irreversible hydrosols. *Proc. R. Soc. London* **1900**, *66*, 110–125.
(24) Tipping, E.; Higgins, D. C. The Effect of Adsorbed Humic Substances on the Colloid Stability of Hematite Particles. *Colloids Surf.* **1982**, *5*, 85–92.
(25) Heidmann, I.; Christl, I.; Kretzschmar, R. Aggregation kinetics of kaolinite-fulvic acid colloids as affected by the sorption of Cu and Pb. *Environ. Sci. Technol.* **2005**, *39*, 807–813.
(26) Illes, E.; Tombacz, E. The effect of humic acid adsorption on pH-dependent surface charging and aggregation of magnetite nanoparticles. *J. Colloid Interface Sci.* **2006**, *295*, 115–123.
(27) Gao, J.; Youn, S.; Hovsepyan, A.; Llaneza, V. L.; Wang, Y.; Bitton, G.; Bonzongo, J. C. J. Dispersion and Toxicity of Selected Manufactured Nanomaterials in Natural River Water Samples: Effects of Water Chemical Composition. *Environ. Sci. Technol.* **2009**, *43*, 3322–3328.
(28) Hou, W. C.; Jafvert, C. T. Photochemical Transformation of Aqueous C-60 Clusters in Sunlight. *Environ. Sci. Technol.* **2009**, *43*, 362–367.
(29) Lee, J.; Cho, M.; Fortner, J. D.; Hughes, J. B.; Kim, J. H. Transformation of Aggregate C-60 in the Aqueous Phase by UV Irradiation. *Environ. Sci. Technol.* **2009**, *43*, 4878–4883.
(30) Smith, B.; Wepasnick, K.; Schrote, K. E.; Cho, H. H.; Ball, W. P.; Fairbrother, D. H. Influence of Surface Oxides on the Colloidal Stability of Multi-Walled Carbon Nanotubes: A Structure−Property Relationship. *Langmuir* **2009**, *25*, 9767–9776.
(31) International Humic Substances Society. http://ihss.gatech.edu/ihss2/elements.html (Accessed April 4, 2010).
(32) Bouchard, D.; Ma, X.; Issacson, C. Colloidal Properties of Aqueous Fullerenes: Isoelectric Points and Aggregation Kinetics of C-60 and C-60 Derivatives. *Environ. Sci. Technol.* **2009**, *43*, 6597–6603.
(33) Smith, B.; Wepasnick, K.; Schrote, K. E.; Bertele, A. H.; Ball, W. P.; O'Melia, C.; Fairbrother, D. H. Colloidal Properties of Aqueous Suspensions of Acid-Treated, Multi-Walled Carbon Nanotubes. *Environ. Sci. Technol.* **2009**, *43*, 819–825.
(34) Wu, W.; Giese, R. F.; van Oss, C. J. Stability versus flocculation of particle suspensions in water - correlation with the extended DLVO approach for aqueous systems, compared with classical DLVO theory. *Colloids Surf., B* **1999**, *14*, 47–55.
(35) Sano, M.; Okamura, J.; Shinkai, S. Colloidal nature of single-walled carbon nanotubes in electrolyte solution: The Schulze-Hardy rule. *Langmuir* **2001**, *17*, 7172–7173.
(36) Elimelech, M.; Gregory, J.; Jia, X.; Williams, R. A. *Particle Deposition and Aggregation: Measurement, Modelling and Simulation*; Oxford, UK, 1995.
(37) Chen, K. L.; Elimelech, M. Interaction of Fullerene (C-60) Nanoparticles with Humic Acid and Alginate Coated Silica Surfaces: Measurements, Mechanisms, and Environmental Implications. *Environ. Sci. Technol.* **2008**, *42*, 7607–7614.
(38) Feng, X. J.; Simpson, A. J.; Simpson, M. J. Chemical and mineralogical controls on humic acid sorption to clay mineral surfaces. *Org. Geochem.* **2005**, *36*, 1553–1566.
(39) Arnarson, T. S.; Keil, R. G. Mechanisms of pore water organic matter adsorption to montmorillonite. *Mar. Chem.* **2000**, *71*, 309–320.
(40) Mariquit, E.; Salim, C.; Hinode, H. The Effect of Calcium Ions in the Adsorption and Photocatalytic Oxidation of Humic Acid. *J. Chem. Eng. Jpn.* **2009**, *42*, 538–543.
(41) Mariquit, E. G.; Salim, C.; Hinode, H. The Role of Calcium Ions in the Photocatalytic Oxidation of Humic Acid at Neutral pH. In *Environmental Challenges in the Pacific Basin*; Carpenter, D. O., Ed.; Blackwell Publishing: Oxford, 2008; Vol. 1140, pp 389−393.

ES101947F